Concomitant Gradient Terms in Phase Contrast MR: Analysis and Correction

Matt A. Bernstein, Xiaohong Joe Zhou, Jason A. Polzin, Kevin F. King, Alexander Ganin, Norbert J. Pelc, Gary H. Glover

Whenever a linear gradient is activated, concomitant magnetic fields with non-linear spatial dependence result. This is a consequence of Maxwell's equations, i.e., within the imaging volume the magnetic field must have zero divergence, and has negligible curl. The concomitant, or Maxwell field has been described in the MRI literature for over 10 years. In this paper, we theoretically and experimentally show the existence of two additional lowest-order terms in the concomitant field, which we call cross-terms. The concomitant gradient cross-terms only arise when the longitudinal gradient G_z is simultaneously active with a transverse gradient (G_x or G_y). The effect of all of the concomitant gradient terms on phase contrast imaging is examined in detail. Several methods for reducing or eliminating phase errors arising from the concomitant magnetic field are described. The feasibility of a joint pulse sequence-reconstruction method, which requires no increase in minimum TE, is demonstrated. Since the lowest-order terms of the concomitant field are proportional to G^2/B_O, the importance of concomitant gradient terms is expected to increase given the current interest in systems with stronger gradients and/or weaker main magnetic fields.

Key words: concomitant gradient terms; concomitant field; Maxwell terms; phase contrast.

INTRODUCTION

Phase contrast angiography (1–5) can depict flow direction and volume flow rate, and also provide angiograms with excellent stationary tissue suppression. Phase contrast images are usually acquired by collecting multiple MRI data sets with different flow sensitivity due to different values of the first gradient moment. The data sets are then individually Fourier transformed, and a phase difference is calculated on a pixel-by-pixel basis, yielding a map where phase is proportional to the velocity component along the direction of the flow-sensitizing gradient.

Phase maps acquired in this manner are subject to systematic errors, e.g., those which arise from gradient eddy currents (6). Phase errors can cause shading artifacts in MR phase contrast angiograms, and erroneous velocity measurements. In this paper we examine the phase errors from a different source: the concomitant magnetic field (7–16). The concomitant magnetic field, or Maxwell field, was first described in the MRI literature over ten years ago. The effect of the concomitant field is small (≤2 ppm at 1.5 T with a gradient amplitude of 10 mT/m and a 20-cm distance from isocenter), and is thus largely neglected in most imaging situations. With the current interest in low-field systems and higher amplitude gradient systems, however, the importance of the concomitant magnetic field increases. In this paper we build on prior work by theoretically and experimentally demonstrating the existence of two cross-terms in the concomitant field. We then explore the effect of the concomitant gradient terms on phase contrast in greater detail. We propose several modifications to the phase contrast pulse sequence that can minimize phase errors from the concomitant field. We then demonstrate a joint pulse sequence-reconstruction method that can effectively correct the concomitant field phase error, with no increase in minimum TE.

MRM 39:300–308 (1998)

From the GE Medical Systems, Waukesha, Wisconsin (M.A.B., X.J.Z., J.A.P., K.F.K., A.G.), and Department of Radiology, Lucas MRS Imaging Center, Stanford University School of Medicine, Stanford, California (N.J.P., G.H.G.).

Address correspondence to: Matt Bernstein, Ph.D., W-875, Applied Science Laboratory, GE Medical Systems, 3200 N. Grandview Boulevard, Waukesha, WI 53188.

Received May 30, 1997; accepted August 7, 1997.

0740-3194/98 $3.00

Copyright © 1998 by Williams & Wilkins
All rights of reproduction in any form reserved.

METHODS

Concomitant Magnetic Field

Whenever a desired linear magnetic field gradient is activated, additional magnetic fields with nonlinear spatial dependence result. This is a consequence of Maxwell's equations for the divergence and curl of the magnetic field. Let the main magnetic field B_0 be oriented in the z direction, and let the applied gradients be G_x, G_y, and G_z, where x, y, and z are the coordinates of a magnet-based frame of reference. Figure 1 illustrates that when there are non-zero components of the field in the x or y direction, the length of the magnetic field vector exceeds the sum of $B_0 + \mathbf{G} \cdot \mathbf{r}$ (where $\mathbf{G} \cdot \mathbf{r} = G_x x + G_y y + G_z z$) by an amount B_C. As derived in Appendix A, the concomitant magnetic field to the lowest order is:

$$B_C(x, y, z, t) = \frac{1}{2B_0}\{G_x^2 z^2 + G_y^2 z^2 + G_z^2 \frac{x^2 + y^2}{4} - G_x G_z xz - G_y G_z yz\} \quad [1]$$

The derivation of the concomitant field expressed in Eq. [1] assumes symmetry of the x and y gradient coils, with a 90° co-axial rotation between them. This assumption is not particularly limiting since it is generally true in commercial MRI systems, including some non-superconducting magnets. A more general expression, including the $1/B_0^2$ order concomitant gradient terms, is given in Appendix A, Eq. [A13].

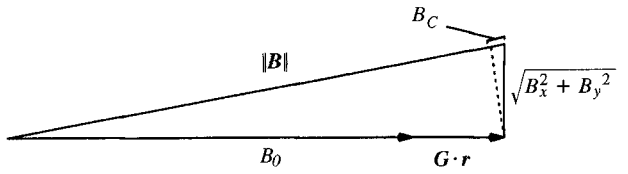

FIG. 1. The concomitant magnetic field B_C is the amount by which the length of the magnetic field vector $\|\mathbf{B}\|$ (the *entire* hypotenuse) exceeds the sum main magnetic field B_0, plus the field from the gradients $\mathbf{G} \cdot \mathbf{r}$. Note that the orientation of the resultant magnetic field is also tipped away from B_0. For illustration purposes, the lengths of $\mathbf{G} \cdot \mathbf{r}$, B_x, B_y, and B_C have been exaggerated.

The concomitant magnetic field of Eq. [1] comprises five terms. We say the first three terms are of the "self-squared" type, since they involve the product of a gradient with itself, such as G_z^2. We call the last two terms concomitant gradient cross-terms since they require the simultaneous activation of the longitudinal and a transverse gradient, such as G_y and G_z. These cross-terms, which have hyperbolic spatial dependence, have not been previously reported to our knowledge, except in our preliminary work (14, 16).

According to Fig. 1, B_C must be non-negative. Despite the signs of the cross-terms, this can be verified by factoring Eq. [1] into the non-negative (assuming $B_0 > 0$) expression:

$$B_C(x, y, z, t) = \frac{1}{2B_0}\left\{\left(G_x z - \frac{G_z x}{2}\right)^2 + \left(G_y z - \frac{G_z y}{2}\right)^2\right\} \quad [2]$$

Effect on Phase Contrast

The phase accumulated by transverse magnetization subjected to the concomitant field is

$$\phi_C(x, y, z) = \gamma \int B_C(x, y, z, t)\, dt \quad [3]$$

With the exception of k-space based complex difference methods (5), phase contrast reconstructions are based on the phase difference operation. The residual concomitant field phase error after the phase difference operation is:

$$\Delta\phi_C(x, y, z) = \phi_{C,fe1}(x, y, z) - \phi_{C,fe2}(x, y, z) \quad [4]$$

where *fe* is the flow encoding index (e.g., "positive or negative bipolar").

The phase difference operation can be accomplished with the following mathematical operation:

$$\Delta\phi(x, y, z) = \arg\left(\frac{Z_{fe1}}{Z_{fe2}}\right) = \arg(Z_{fe1}\, Z^*_{fe2}) \quad [5]$$

where Z_{fe1} and Z_{fe2} are complex images after Fourier transformation of the *fe*1 and *fe*2 data sets respectively, * denotes complex conjugate, and "arg" represents the phase of a complex number, i.e., $\arg(z) = \tan^{-1}(Im(z)/Re(z))$. Equation [5] can be modified to account for multicoil data (17).

Artifact Reduction Strategies

Shading artifacts result when the desired phase difference $\Delta\phi$ (Eq. [5]) is contaminated by the concomitant field phase error $\Delta\phi_C$ (Eq. [3]). There are two main strategies to reduce or eliminate these artifacts. In the first strategy, the source of the concomitant field phase error $\Delta\phi_C$ is reduced by gradient waveform design. This strategy can be effective, but there is inevitably a penalty in minimum TE, which usually also translates to an increase in minimum TR. In the second strategy, a phase correction is applied in the image domain during the reconstruction process.

As can be seen from Eqs. [1] and [3], the use of anti-symmetric gradient lobes ($G(fe_1) = -G(fe_2)$) for flow encoding eliminates phase errors from self-squared terms (like G_x^2). This was first pointed out by Norris and Hutchison (9). The use of anti-symmetric lobes, however, does not necessarily null phase errors arising from the cross-terms ($G_z G_x$ and $G_z G_y$), as illustrated by Figure 2a. Moreover, the performance penalty for playing anti-symmetric lobes rather than combined lobes can be substantial; quantitative examples are given in Tables 1 and 2 of Reference 18.

Playing G_z nonconcurrently with G_x and G_y, in addition to using antisymmetric lobes (Fig. 2b), is guaranteed to eliminate phase errors arising from all five concomitant gradient terms (Eq. [1]), but the minimum TE penalty is even greater than the use of anti-symmetric lobes alone. Note that some six-set encoding schemes (5) have

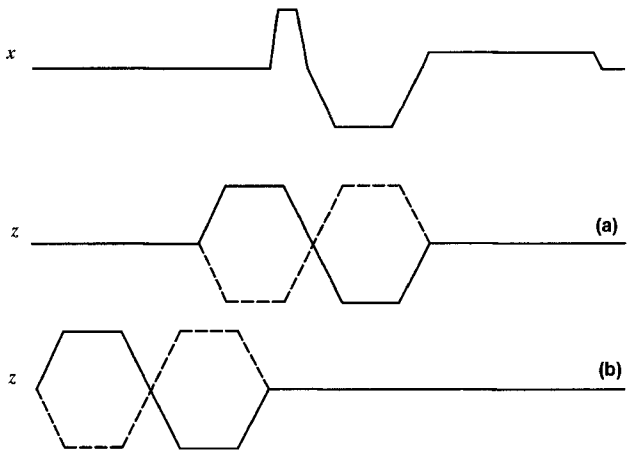

FIG. 2. Although anti-symmetric bipolar flow encoding lobes insure cancellation of the phase from self-squared concomitant gradient terms like G_z^2, they do not insure cancellation of cross-terms like $G_x G_z$. Consider the following example: a) The bipolar pair on the *z* axis (solid line) has a net positive overlap integral with the readout waveform on *x*. For the second flow encode (dashed line), the overlap integral is negative. When the two are subtracted in accordance with Eq. [7c], the errors accumulate, rather than cancel. b) If the bipolar lobes are not only anti-symmetric, but also are played when $G_x = 0$, then the concomitant field phase errors with x^2, y^2 and xz spatial dependence are all guaranteed to be zero. The waveform design in (b), however increases minimum TE and TR by an unacceptable amount for many applications.

favorable concomitant field phase properties, but their acquisition efficiency is also lower.

A final pulse sequence-based strategy is to de-rate the maximum amplitude of the gradient lobes. This also increases minimum TE and TR (18, 19). Appendix B shows that for a trapezoidal lobe with fixed area, the accumulated concomitant field phase is approximately proportional to the maximum gradient amplitude.

An alternative strategy is to correct the concomitant field phase error in the image domain. In this approach the correction is applied by the reconstruction program.

The concomitant field phase error, like phase errors arising from gradient eddy currents, can be fitted to a polynomial. If u and v are the readout and phase encode directions, respectively, then in general the concomitant field phase error can have the following spatial dependence:

$$\Delta\phi(u, v) = \alpha u + \beta v + \gamma u^2 + \delta v^2 + \epsilon uv + \zeta \quad [6]$$

The coefficients α, β, γ, δ, ϵ, and ζ can be determined with linear regression (20). Equation [6] can be verified by first considering the spatial dependence of the quadratic form in Eq. [1], and then applying an arbitrary rotation (for obliques) and translation (for off-center field of view or slice offset). Although the spatial dependence of the concomitant field in Eq. [1] is purely quadratic in the magnet-based coordinates, in the image coordinates u and v it can produce linear (e.g., αu), and even constant (i.e., ζ) phase errors.

One advantage of this least squares method is that both the eddy current and concomitant field corrections can be accomplished in a single step. Its main disadvantage, however, is contamination to the fit from the desired, flow-related phase. Thus, we recommend the following method instead.

Joint Pulse Sequence-Reconstruction Correction

Since the pulse sequence program has detailed information about the gradient waveforms, it can calculate the coefficients of the phase error, and pass them to the reconstruction program. The reconstruction program can then apply the phase correction in the image domain. Figure 3 illustrates a flowchart for this method. The remainder of this paper focuses on the implementation and validation of this method.

As indicated in Fig. 3, the gradient waveforms are transformed from the read-phase-slice to x, y, z coordinate systems with point-by-point multiplication by the orthogonal rotation matrix. From Eqs. [1]–[3], the next step is for the pulse sequence program to calculate the coefficients:

$$A = \frac{\gamma}{2B_0}\int \{(G_x^2(t) + G_y^2(t))_{fe1} - (G_x^2(t) + G_y^2(t))_{fe2}\}dt \quad [7a]$$

$$B = \frac{\gamma}{8B_0}\int \{G_z^2(t)_{fe1} - G_z^2(t)_{fe2}\}\, dt \quad [7b]$$

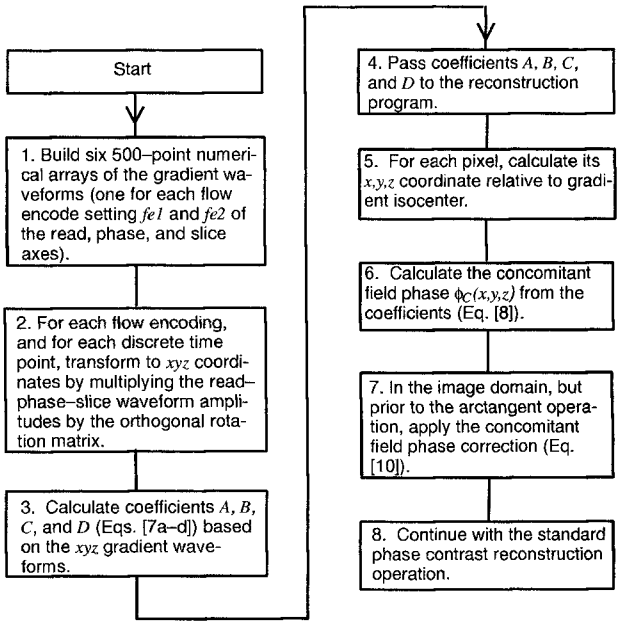

FIG. 3. Flow chart for the joint pulse sequence-reconstruction concomitant field correction described in Methods.

$$C = -\frac{\gamma}{2B_0}\int \{[G_x(t)\ G_z(t)]_{fe1} - [G_x(t)\ G_z(t)]_{fe2}\}\, dt \quad [7c]$$

$$D = -\frac{\gamma}{2B_0}\int \{[G_y(t)\ G_z(t)]_{fe1} - [G_y(t)\ G_z(t)]_{fe2}\}\, dt \quad [7d]$$

The integrals in Eqs. [7a]–[7d] are evaluated over a time interval which includes all the gradient lobes that change between the two flow encodes. The *fe*1 and *fe*2 contributions to Eqs. [7a]–[7d] from all remaining time intervals cancel. Usually the required time interval extends from the end of the slice selection plateau to the beginning of the readout plateau. We call this time interval t_C. Since the phase-encoding gradient (and slice gradient for 3D) is incremented, a single value (i.e., k-space location) must be selected to calculate Eqs. [7a]–[7d]. We choose the step that corresponds to the center of k-space. The calculated concomitant field phase error can then be expressed in terms of the calculated coefficients, and the magnet-based spatial coordinates:

$$\Delta\phi_C(x, y, z) = A\, z^2 + B(x^2 + y^2) + C\, xz + D\, yz \quad [8]$$

Under some circumstances, the integrals in Eqs. [7a]–[7d] can be calculated analytically. For example, a trapezoidal lobe with amplitude Go, plateau duration F, and two equal ramp durations r has a simple expression for its

self-squared integral:

$$M = \int G^2(t)\, dt \qquad [9]$$

$$= G^2_0\left(F + \frac{2}{3} r\right) \text{ [trapezoidal lobe]}$$

Thus, for trapezoidal lobes, the coefficients A and B can be expressed as a difference between two expressions of the form of Eq. [9]. Unfortunately the cross-term coefficients C and D have no such simple expressions. Therefore we instead choose to evaluate Eqs. [7a]–[7d] numerically in the pulse sequence program by forming a discrete representation of the gradient waveforms over the time interval t_C. A further advantage of this numerical method is that the orthogonal rotation matrix can be applied to each time point of the read, phase, and slice waveforms, so the method remains valid regardless of the oblique orientation.

The pulse sequence program then passes the calculated coefficients A, B, C, and D to the reconstruction process so that it can calculate the concomitant field phase using Eq. [8]. The reconstruction program must determine the x, y, and z coordinates for each pixel in the image. On our imaging system, this information is available to the reconstruction program (as part of the gradient non-uniformity correction (21, 22)) via three image "corner point" vectors.

Once the x, y, and z coordinates of each pixel are determined, the concomitant field phase is calculated with Eqs. [7] and [8]. The concomitant field phase is corrected *before* the arctangent (arg) operation, which avoids problems in regions of 2π phase wrap. To apply the concomitant field phase correction prior to calculating the arctangent, the standard phase difference operation of Eq. [5] is replaced by

$$\Delta\phi_{\text{corr}}(x, y, z) = \arg\left(\frac{Z_{fe1}}{Z_{fe2}} e^{-i\Delta\phi_C(x,y,z)}\right) \qquad [10]$$

$$= \arg(Z_{fe1}(Z_{fe2})^* e^{-i\Delta\phi_C(x,y,z)})$$

If additional phase correction for eddy current-induced phase errors is required, it may be applied to the result of Eq. [10]. If images in all three flow directions are acquired (either with four or six-set methods), then each flow direction image receives an independent concomitant field correction.

If concomitant field correction for a complex difference (CD) reconstruction is desired, then the corrected phase difference in Eq. [10] is used in conjunction with the Law of Cosines to calculate the complex difference in the image domain:

$$CD_{\text{corr}} = \sqrt{|Z_{fe1}|^2 + |Z_{fe2}|^2 - 2|Z_{fe1}|\,|Z_{fe2}|\cos(\Delta\phi_{\text{corr}}(x, y, z))} \qquad [11]$$

RESULTS

We implemented the joint pulse sequence-reconstruction method on GE HiSpeed Horizon scanners (GE Medical Systems, Milwaukee, WI) running either version 5.6 or 8.1 software. We have corrected approximately 100 images using the joint pulse sequence-reconstruction method. Figure 4 shows a representative plot of measured phase versus z, similar to those shown in refs. 9 and 10. Here the G_y gradient is causing a z^2 phase error. The field of view is 32 cm, the slice thickness is 10 mm, the aliasing velocity VENC = 5 cm/s, and B_O = 1.5 T. The maximum gradient amplitude is 22 mT/m, and the slew rate is 77 T/m/s. (Gradients with the same specifications were used to acquire all the data reported in this paper.) The solid line has a coefficient A = 0.499°/cm, which is calculated from the specific gradient waveforms and Eq. [7a], with no adjustable parameters.

Figure 5a shows a 40-cm sagittal image of a stationary phantom with A/P flow encoding, acquired at B_O = 1.0 T, VENC = 5 cm/s, TR = 33 ms, and TE = 9.0 ms. For the particular waveforms used, Eq. [7d] predicts a yz cross-term phase error with the coefficient D = 1.45°/cm^2. Since the flow encoding gradient lobes were antisymmetric, the phase errors from the self-squared concomitant gradient terms are zero. The hyperbolic yz spatial dependence of the phase error is apparent from Fig. 5a. Figure 5b shows the image corrected according to Eq. [10]. Note how the yz-phase error is reduced, and also that the former 2π wrap boundaries are now smooth. Quantitatively, the standard deviation within a centered, 27-cm circular region of interest (ROI) covering the phantom was reduced from 62° to 13°. The maximum deviation of the phase (from the correct value of zero) was reduced from 103° to 22° within the ROI. No correction for eddy current-related phase errors was applied. Note that the concomitant field phase error dominates the eddy current-related phase error in this instance.

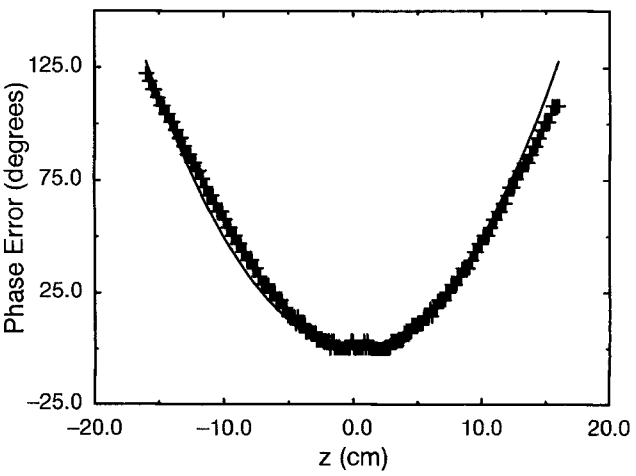

FIG. 4. Validation of the calculated concomitant field phase error. The +'s represent the measured phase error, and the solid line represents the calculated concomitant field phase, with zero adjustable parameters. The field strength is 1.5 T, a 10-mm-thick coronal slice is used, and A/P flow sensitizing gradients were applied such that aliasing velocity VENC = 5 cm/s.

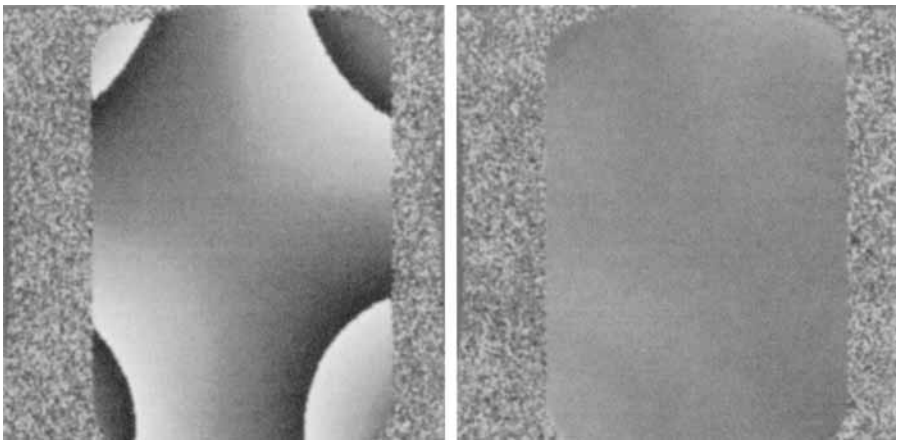

FIG. 5. 40-cm field of view sagittal phase difference images of a stationary phantom illustrating the *yz* concomitant gradient cross-term, and the proposed joint pulse sequence-reconstruction correction method. a) No concomitant field correction. b) Concomitant field correction. See text.

Figure 6a shows a maximum intensity projection (MIP) of four 20-mm thick complex difference coronal slabs of a normal volunteer acquired at B_O = 1.0 T. The field of view is 32 cm, VENC = 25 cm/s, TR = 33 ms, and TE = 7.1 ms. The concomitant field correction (Fig. 6b) removes a z^2 phase error that leads to shading in the neck, and also near the top of the head. Correcting the $x^2 + y^2$ phase removes shading which outlines the ears. Although the concomitant field is zero at the gradient isocenter, the concomitant field correction even reduces the background level of stationary tissue from 60 ± 12 to 45 ± 10, for a 2-cm ROI centered near $x = y = z = 0$. We believe this is because an eddy current correction was applied to both Figs. 6a and 6b. If uncorrected, the concomitant field phase (and especially its z^2 spatial dependence) can cause an error in the least squares fit of the constant term, such as ζ in Eq. [6].

Performance

There are two performance issues to consider with the joint pulse sequence-reconstruction concomitant field correction: 1) the time penalty for calculating the coefficients *A*, *B*, *C*, and *D* in the pulse sequence program, and 2) the time penalty for applying the phase correction to the image during reconstruction. The pulse sequence time penalty depends on the number of discrete points used to numerically evaluate the integrals in Eq. [7]. We find that 500 points typically yields less than 0.5% error in the coefficients *A*, *B*, *C*, and *D* for a time interval $t_C \approx 5$ ms. The calculation time with 500 points is less than 200 ms with a 68040 processor (Motorola, Inc. Schaumburg, IL). The additional reconstruction time to apply the correction to three 256 × 256 phase difference images representing the three flow directions is approximately 150 ms using four parallel i860 array processors (Mercury Computer Systems Inc., Chelmsford, MA). Note that the reconstruction time penalty of the concomitant field correction is essentially independent of the number of phased-array multicoil channels, since the concomitant field correction is applied in the image domain, after the multicoil combination (17).

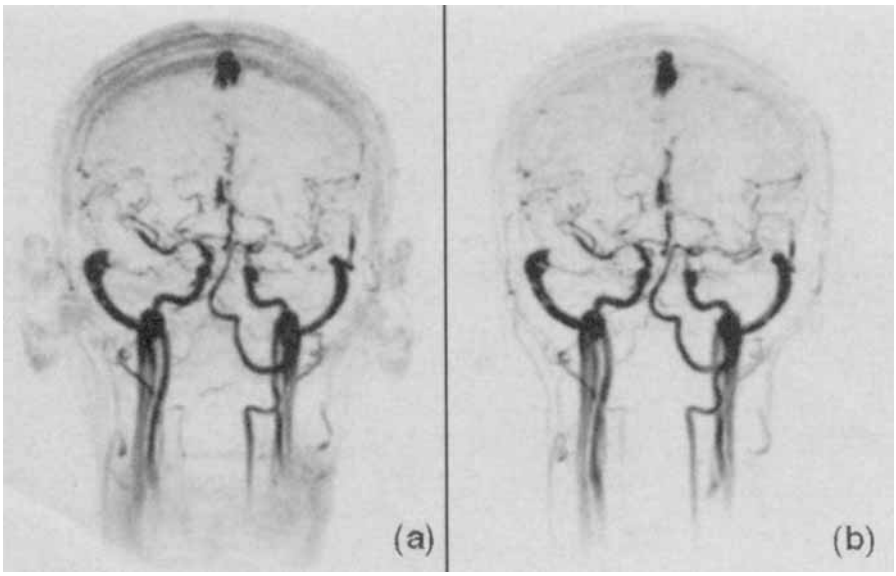

FIG. 6. Coronal complex difference images of a normal volunteer. TR = 33 ms, TE = 7.1 ms, 32 cm field of view, MIP of four 20-mm thick contiguous slabs, 512 × 192, 4-set flow encoding yielding flow sensitivity to all directions, 3 signal averages, scan time 5 min, 10 s. a) No concomitant field correction, b) concomitant field correction.

DISCUSSION

Phase Contrast and Other Phase Sensitive Techniques

Like eddy currents, the concomitant magnetic field affects the most phase sensitive imaging techniques. In our experience these techniques include phase contrast, echo planar imaging (EPI), spirals, RARE (and its variants, such as fast spin echo), GRASE, and spectroscopy. In this paper we concentrated on phase contrast since it gives a direct spatial map of the phase errors, thereby making it easy to separately measure the concomitant gradient terms and their spatial dependencies. We also have investigated the effects of the concomitant field on EPI, spirals, and fast spin echo, and the results will be reported soon.

Concomitant Magnetic Fields and Eddy Currents

It may be worthwhile to compare the concomitant magnetic field to the fields induced by gradient eddy currents. Gradient eddy currents are caused by gradient slewing, while concomitant fields are caused by gradient amplitude (i.e., current). Fields induced by eddy currents normally have constant and linear spatial dependence, while the lowest order concomitant gradient terms have quadratic spatial dependence. Eddy currents are characterized by one or more exponential decay time constants, while concomitant gradient terms vanish with the applied gradient. The severity of the gradient eddy currents is related to the design and manufacture of the gradient coil, RF shield, cryostat (if present), and other hardware, while the concomitant field of Eq. [A13] is a fundamental physics effect, and is therefore hardware independent.

Despite these differences, it is possible to mistake concomitant gradient terms for eddy currents. This may be especially true with the concomitant gradient cross-terms given in Eq. [1]. Consider, for example, an offset sagittal slice, described by the equation $x = x_O$. In this case the xz-concomitant gradient cross-term

$$B_C = -\frac{G_x G_z x_0}{2B_0} z \qquad [12]$$

could easily be mistaken for a linear z eddy current. This concomitant gradient term, however, has a distinguishing property that it is only present when both the x and z gradients are active.

Thick Slices

The joint pulse sequence-reconstruction correction described by Eqs. [7], [8], and [10] in Methods has relatively few drawbacks. One drawback is moderate engineering complexity, but this can be overcome. A more fundamental drawback arises with the use of thick slices, or slabs, such as those commonly used in complex difference phase contrast angiograms. They are problematic since the magnet x, y, and z coordinates along the slice direction can vary. The corner point vectors of a thick slab are normally chosen to represent the slice coordinate at the center of the slab. Often in thick slab angiography, however, we image small vessels that may lie at any location within the slab.

In our experience this potential drawback for thick slab angiography has not proved too limiting. We speculate, however, in some cases optimal performance of the concomitant field correction might require combination with some gradient amplitude de-rating for thick slabs ($\gtrsim$20 mm). This is an area of further study.

Vertical-Field Magnet Geometry

Since the concomitant field of Eq. [1] has $1/B_0$ field dependence its importance increases for low-field systems. Many commercial low-field systems employ vertical-field geometry. The derivations and discussion given in this paper are valid for vertical-field magnet geometries as well as the conventional cylindrical geometry employed with superconducting systems. It is important to remember, however, that for vertical-field geometry the z axis corresponds to the anterior/posterior axis in the patient. This has the consequence that for a given flow encoding direction, e.g., anterior/posterior, the calculated values of the coefficients in Eq. [7] differ for the two magnet geometries, even at the same B_0.

For extremely low fields, concomitant gradient terms of order $(1/B_0)^2$ can be non-negligible. For this reason, we carried the derivation of Eq. [A13] in Appendix A to that order.

Gradient Non-Uniformity Terms

The derivation of Eq. [A13] assumes perfect gradient uniformity. Especially for larger fields of view (e.g., $\gtrsim$32 cm) a gradient non-uniformity correction (21, 22) may be required since the actual gradient is often weaker than the nominal value far from gradient isocenter. The actual spatial dependence of the gradient relies on its design and manufacture, so here we draw only general conclusions about the effect of gradient non-uniformity.

Gradient non-uniformity manifests itself in non-zero higher order derivatives in Eq. [A1]. For example, from Eqs. [A1]–[A3] the expansion of the magnetic field vector $\mathbf{B}$ contains second-order terms like

$$x\, z \frac{\partial^2 \mathbf{B}}{\partial x \partial z} = x\, z \frac{\partial \mathbf{G}}{\partial x} \qquad [13]$$

If the Taylor expansion in Eq. [A1] is performed about the gradient isocenter, then from gradient symmetry, we expect the even-order derivatives of $\boldsymbol{B}$, such as the one shown in Eq. [13] to be negligible. If the expansion is performed about a point offset from the origin, this symmetry no longer holds, and we expect that the even-order derivatives can be non-negligible. Note that unlike concomitant gradient terms, the gradient non-uniformity terms are independent of B_O. In our experience the gradient non-uniformity terms are negligible for fields of view less than 32 cm. Quantifying these terms is another area of further study.

CONCLUSION

The concomitant magnetic field can have non-negligible effects on phase-sensitive imaging techniques such as phase contrast. We theoretically and experimentally demonstrated the existence of concomitant gradient cross-terms, which are of order $1/B_0$. We discussed several gradient waveform design strategies that reduce the concomitant field phase error, at the cost of increasing minimum TE. We then presented, and demonstrated the feasibility of a joint pulse sequence-reconstruction method that reduces the concomitant field phase error with no penalty in minimum TE.

APPENDIX A

Here we derive the concomitant magnetic field up to cubic spatial dependence, including cross-terms. The

concomitant field can be determined with a vector Taylor expansion [23]

$$\boldsymbol{B} - B_0\,\boldsymbol{k} = (\boldsymbol{r}\cdot\nabla)\boldsymbol{B} + \left(\frac{x^2}{2}\frac{\partial^2}{\partial x^2} + \frac{y^2}{2}\frac{\partial^2}{\partial y^2} + \frac{z^2}{2}\frac{\partial^2}{\partial z^2} + xy\frac{\partial^2}{\partial x\,\partial y} + xz\frac{\partial^2}{\partial x\,\partial z} + yz\frac{\partial^2}{\partial y\,\partial z}\right)\boldsymbol{B}\ldots \quad [A1]$$

where boldface type symbols represent vectors, and $\boldsymbol{k}$ is a unit vector in the z direction. The first term of Eq. [A1] can be re-cast from vector form into a more explicit matrix form:

$$\begin{bmatrix} B_x \\ B_y \\ B_z - B_0 \end{bmatrix} = \begin{bmatrix} \frac{\partial B_x}{\partial x} & \frac{\partial B_x}{\partial y} & \frac{\partial B_x}{\partial z} \\ \frac{\partial B_y}{\partial x} & \frac{\partial B_y}{\partial y} & \frac{\partial B_y}{\partial z} \\ \frac{\partial B_z}{\partial x} & \frac{\partial B_z}{\partial y} & \frac{\partial B_z}{\partial z} \end{bmatrix} \begin{bmatrix} x \\ y \\ z \end{bmatrix} + \ldots \quad [A2]$$

Since there are three components of $\boldsymbol{B}$, and three spatial coordinates, Equation [A2] contains a total of nine partial derivatives. The partial derivatives of B_z are recognized to be the desired imaging gradients:

$$\begin{bmatrix} B_x \\ B_y \\ B_z - B_0 \end{bmatrix} = \begin{bmatrix} \frac{\partial B_x}{\partial x} & \frac{\partial B_x}{\partial y} & \frac{\partial B_x}{\partial z} \\ \frac{\partial B_y}{\partial x} & \frac{\partial B_y}{\partial y} & \frac{\partial B_y}{\partial z} \\ G_x & G_y & G_z \end{bmatrix} \begin{bmatrix} x \\ y \\ z \end{bmatrix} + \ldots \quad [A3]$$

Like previous authors (7–13), we assume that the true and displacement current densities are negligible within the imaging volume, so that $\nabla \times \mathbf{B} = \mathbf{0}$ (23). The x, y, and z components of this curl equation, respectively, yield

$$\frac{\partial B_y}{\partial x} = \frac{\partial B_x}{\partial y} \equiv g \quad [A4]$$

$$\frac{\partial B_y}{\partial z} = \frac{\partial B_z}{\partial y} = G_y \quad [A5]$$

$$\frac{\partial B_x}{\partial z} = \frac{\partial B_z}{\partial x} = G_x \quad [A6]$$

Equations [A5] and [A6] specify two of the six undetermined partial derivatives in Eq. [A3]. Two of the remaining unspecified derivatives are given by the parameter g in Eq. [A4]. Unlike the other seven, these two derivatives are neither a desired gradient, nor are they coupled to a desired gradient by any of Maxwell's equations. Therefore it is reasonable to assume that g is zero. Note that Maxwell's equations do not force g to be zero, but rather in the absence of a gradient coil which generates it, g will remain zero. With the gradient system we used to obtain the results reported here, calculated field plots show $g/G_z < 2\%$ over a spherical volume of radius 20 cm. For generality, however, we carry the parameter g through Eq. [A13].

The divergence equation for the magnetic field (23) further requires:

$$\frac{\partial B_x}{\partial x} + \frac{\partial B_y}{\partial y} + \frac{\partial B_z}{\partial z} = \frac{\partial B_x}{\partial x} + \frac{\partial B_y}{\partial y} + G_z = 0 \quad [A7]$$

We introduce a dimensionless symmetry parameter α, which specifies the two remaining partial derivatives in Eq. [A3]:

$$\frac{\partial B_x}{\partial x} \equiv -\alpha\, G_z \quad [A8]$$

From the divergence constraint (Eq. [A7]), the symmetry parameter α also must satisfy the relation

$$\frac{\partial B_y}{\partial y} = G_z(\alpha - 1) \quad [A9]$$

All the MRI systems with which we are familiar have cylindrical symmetry, which requires $\alpha = 0.5$. To avoid loss of generality, however, we shall retain the general symmetry parameter α throughout the remainder of the derivation.

Substituting Eqs. [A4], [A8], and [A9] into Eq. [A3] yields

$$\begin{bmatrix} B_x \\ B_y \\ B_z - B_0 \end{bmatrix} = \begin{bmatrix} -\alpha G_z & g & G_x \\ g & (\alpha - 1)G_z & G_y \\ G_x & G_y & G_z \end{bmatrix} \begin{bmatrix} x \\ y \\ z \end{bmatrix} + \ldots \quad [A10]$$

From Eq. [A10] (if we neglect gradient non-uniformities, and assume g is at least spatially constant, if not zero) we can conclude that all nine of the first derivatives of the field (i.e., the matrix elements) are spatially constant. Thus for perfectly uniform gradients, the second and higher order derivatives of the magnetic field are zero, and the expansion given in Eq. [A1] has no terms beyond $(\mathbf{r}\cdot\nabla)\mathbf{B}$. The Discussion section further addresses the question of gradient non-uniformity.

We calculate the length of the magnetic field vector, since it is the quantity that governs the Larmor frequency. (The slight nutation of magnetic field vector away from the z axis might also be of interest. It is straightforward to show, however, that for clinically available gradient amplitudes and slew rates the adiabatic condition (24) is met by a wide margin, so that the slight nutation of the magnetization vector is reversed as soon as the gradient is deactivated.) The Taylor series expansion

$$\sqrt{1+u} = 1 + \frac{1}{2}u - \frac{1}{8}u^2 + \frac{1}{16}u^3 - \ldots \quad [A11a]$$

in conjunction with the substitution

$$u = \frac{B_x^2 + B_y^2}{B_0^2} + 2\frac{\boldsymbol{G}\cdot\boldsymbol{r}}{B_0} + \left(\frac{\boldsymbol{G}\cdot\boldsymbol{r}}{B_0}\right)^2 \qquad \text{[A11b]}$$

yields

$$\|\boldsymbol{B}(x, y, z)\| = \sqrt{B_x^2 + B_y^2 + B_z^2}$$

$$= B_0 + \boldsymbol{G}\cdot\boldsymbol{r} + \frac{B_x^2 + B_y^2}{2\,B_0} - \frac{\boldsymbol{G}\cdot\boldsymbol{r}\,(B_x^2 + B_y^2)}{2\,B_0^2}$$

$$+ \ldots \qquad \text{[A12]}$$

Note cancellation of the $(\mathbf{G}\cdot\mathbf{r})^2$ term in Eq. [A12] requires the expansion of the square root to the second order, i.e., to retain the $-1/8\ u^2$ term in Eq. [A11a]. Substituting expressions for the magnetic field components (Eq. [A10]) into Eq. [A12], and neglecting gradient non-uniformity, yields:

$$\|\boldsymbol{B}(x, y, z)\| = B_0 + \boldsymbol{G}\cdot\boldsymbol{r} +$$

$$+ \frac{1}{2B_0}((\alpha^2G_z^2 + g^2)x^2 + ((\alpha - 1)^2G_z^2 + g^2)y^2$$

$$+ (G_x^2 + G_y^2)z^2)$$

$$+ \frac{1}{B_0}(-gG_zxy + (gG_x + (\alpha - 1)G_yG_z)yz$$

$$+ (gG_y - \alpha G_xG_z)xz)$$

$$- \frac{1}{2B_0^2}(G_x(\alpha^2G_z^2 + g^2)x^3 + G_y((\alpha - 1)^2G_z^2$$

$$+ g^2)y^3 + G_z(G_x^2 + G_y^2)z^3)$$

$$- \frac{1}{2B_0^2}((G_y(\alpha^2G_z^2 + g^2) - 2gG_xG_z)x^2y$$

$$+ (G_z(\alpha^2G_z^2 + g^2) + 2G_x(gG_y$$

$$- \alpha G_xG_z))x^2z)$$

$$- \frac{1}{2B_0^2}(G_x(\alpha - 1)^2G_z^2 + g^2G_x - 2gG_yG_z)xy^2$$

$$- \frac{1}{2B_0^2}((\alpha - 1)^2G_z^3 + g^2G_z + 2G_y(gG_x$$

$$+ (\alpha - 1)G_yG_z))y^2z$$

$$- \frac{1}{2B_0^2}(G_x(G_x^2 + G_y^2) + 2G_z(gG_y$$

$$- \alpha G_xG_z))xz^2$$

$$- \frac{1}{2B_0^2}(G_y(G_x^2 + G_y^2) + 2G_z(gG_x + (\alpha$$

$$- 1)G_yG_z))yz^2$$

$$- \frac{1}{B_0^2}(g(G_x^2 + G_y^2 - G_z^2) - G_xG_yG_z)xyz + \ldots$$

[A13]

Setting $\alpha = 0.5$ and $g = 0$, as justified above, and comparing Eqs. [A12] and [A13], yields the result for the concomitant field to order $1/B_0$, which is given by Eq. [1].

In this investigation we used field strength $B_0 \geq 1.0$ T so that the $(1/B_0)^2$ order concomitant gradient terms in Eq. [A13] are negligible. These terms, however, can become substantial for smaller B_0. For completeness we carried Eq. [A13] to that order, and these terms have interesting properties. As seen from Eq. [A12] and as pointed out in ref. 12, even a lone gradient (e.g., G_x) can produce a term with mixed spatial dependence (e.g., z^2x). Also note the $G_x\,G_y\,G_z$ term, which requires all three gradients to be active, and which produces a field with $x\,y\,z$ spatial dependence.

APPENDIX B

Here we derive scaling relationships between accumulated concomitant field phase from a gradient lobe and the gradient specifications h (maximum amplitude) and r (rise time from 0 to h).

Consider a gradient lobe with area a which exceeds the product $h \times r$. The most efficient way to produce such a lobe is as a slew-rate limited trapezoid. The width w of the trapezoid (including ramps) is given by (18)

$$w = \frac{a}{h} + r \qquad \text{[B1]}$$

The Maxwell self-squared integral is given by Eq. [9], which can be expressed as:

$$M = h^2\left((w - 2r) + \frac{2r}{3}\right) \qquad \text{[B2]}$$

Substituting Eq. [B1] into Eq. [B2] we find

$$M = ha - \frac{h^2r}{3} \qquad \text{[B3]}$$

Since $a > hr$, we can assume $a \gg hr/3$, from which we obtain

$$M \approx ha \qquad \text{[B4]}$$

We assume a is determined by imaging requirements (field of view, slice thickness, aliasing velocity VENC, etc.), so it is fixed. The accumulated concomitant field phase is approximately proportional to the maximum gradient amplitude h. (As described in Methods, cancellation of M can occur when the two flow encoding waveforms of a phase contrast acquisition are considered, but we exclude that possibility in this general discussion.) Thus de-rating the maximum gradient amplitude can be an effective strategy to reduce concomitant field phase errors, although it does prolong the minimum TE.

The approximate linear dependence of the concomitant field phase on h in Eq. [B4] is the result of the G^2 dependence of the self-squared concomitant gradient terms, and the approximate $1/G$ dependence of the duration of the gradient lobe, when its area is fixed.

Next consider a slew rate limited triangular lobe, which is efficient when $a < hr$. Its width and area are related by (18):

$$w = 2\sqrt{\frac{ar}{h}} \qquad [B5]$$

Let the gradient amplitude of the triangle be G_o. We have

$$M = G_o^2\left(\frac{2}{3}\frac{w}{2}\right) \qquad [B6]$$

where slew-rate limited ramps require

$$G_o = \frac{wh}{2r} \qquad [B7]$$

Combining Eqs. [B5]–[B7], we conclude

$$M = \frac{2}{3}\frac{a^{(3/2)}}{\sqrt{\mathrm{SR}}} \qquad [B8]$$

where SR = h/r is the slew-rate limit. Because of the slower square root dependence in Eq. [B8], de-rating SR is a relatively poor strategy to reduce concomitant field phase error compared to de-rating the maximum amplitude h. It should be emphasized that larger lobes cause most of the concomitant field phase errors, so Eq. [B4] is generally a more applicable result than Eq. [B8].

ACKNOWLEDGMENTS

The authors thank Mike Hartley, who helped greatly with the implementation of the reconstruction program, and Takao Goto-san for useful discussions about vertical-field systems.

REFERENCES

1. P. R. Moran, A flow zeugmatographic interface for NMR imaging in humans. *Magn. Reson. Imaging* **1,** 197–203 (1982).
2. D. J. Bryant, J. A. Payne, D. N. Firmin, D. B. Longmore, Measurement of flow with NMR using a gradient pulse and phase difference technique. *J. Comput. Assist. Tomogr.* **8,** 588–593 (1984).
3. M. O'Donnell, NMR blood flow imaging using multiecho, phase contrast sequences. *Med. Phys.* **12,** 59–64 (1985).
4. G. L. Nayler, D. N. Firmin, D. B. Longmore, Blood flow imaging by cine magnetic resonance. *J. Comput. Assist. Tomogr.* **10,** 715–722 (1986).
5. C. L. Dumoulin, S. P. Souza, M. F. Walker, W. Wagle, Three-dimensional phase contrast angiography. *Magn. Reson. Med.* **9,** 139–149 (1989).
6. P. Jehenson, M. Westphal, N. Schuff, Analytical method for the compensation of eddy-current effects induced by pulsed magnetic field gradients in NMR systems. *J. Magn. Reson.* **90,** 264–278 (1990).
7. D. G. Norris, Phase errors in NMR images, *in* "Proc., SMRM, 4th Annual Meeting, 1985," p. 1037.
8. R. Coxon, P. Mansfield, EPI spatial distortion in non-transverse planes, *in* "Proc., SMRM, 8th Annual Meeting, 1989," p. 361.
9. D. G. Norris, J. M. S. Hutchison, Concomitant magnetic field gradients and their effects on imaging at low magnetic field strengths. *Magn. Reson. Imaging* **8,** 33–37 (1990).
10. R. M. Weisskopff, J. J. Dalcanton, R. R. Rzedzian, Image distortion in coronal instant images?, *in* "Proc., SMRM, 9th Annual Meeting, 1990," p. 457.
11. R. M. Weisskopff, M. S. Cohen, R. R. Rzedzian, Nonaxial whole-body instant imaging. *Magn. Reson. Med.* **29,** 796–803 (1993).
12. T. Classen-Vujcic, J. Slotboom, A. F. Mehlkopf, Reduction of the concomitant field gradient effects by main magnetic field alteration, *in* "Proc., SMR, 3rd Annual Meeting, Nice, France, 1995," p. 315.
13. T. Classen-Vujcic, K. Blom, A. F. Mehlkopf, Hardware corrections of concomitant field gradients, *in* "Proc., ISMRM, 5th Annual Meeting, 1997," p. 56.
14. M. A. Bernstein, X. Zhou, K. F. King, A. Ganin, N. Pelc, G. Glover, Shading artifacts in phase contrast angiography induced by Maxwell terms: analysis and correction, *in* "Proc., ISMRM, 5th Annual Meeting, 1997," p. 110.
15. S. E. Maier, O. Heid, A. Jolesz, Flow calibration on an open MR system, *in* "Proc., ISMRM, 5th Annual Meeting, 1997," p. 1872.
16. K. F. King, A. Ganin, X. Zhou, M. A. Bernstein, Effect of Maxwell fields on spiral scans, *in* "Proc., ISMRM, 5th Annual Meeting, 1997," p. 1917.
17. M. A. Bernstein, M. Grgic, T. J. Brosnan, N. J. Pelc, Reconstructions of phase contrast, phased array multicoil data. *Magn. Reson. Med.* **32,** 330–334 (1994).
18. M. A. Bernstein, A. Shimakawa, N. J. Pelc, Minimizing TE in moment-nulled or flow encoded two- and three-dimensional gradient echo imaging. *J. Magn. Reson. Imaging* **2,** 583–588 (1992).
19. S. B. Reeder, E. R. McVeigh, The effect of high performance gradients on fast gradient echo imaging. *Magn. Reson. Med.* **32,** 612–621 (1994).
20. M. A. Bernstein, N. J. Pelc, Phase correction of complex difference processed MR angiograms. US Patent 5,226,418 (1993).
21. K. Sekihara, M. Kuroda, H. Kohno, Image restoration from non-uniform magnetic field influence for direct Fourier imaging. *Phys. Med. Biol.* **29,** 15–24 (1984).
22. G. H. Glover, N. J. Pelc, Method for correction image distortion due to gradient non-uniformity. US Patent 4,591,789 (1986).
23. J. D. Jackson, "Classical Electrodynamics," 2nd ed. Wiley, New York, 1975.
24. A. Abragam, "Principles of Nuclear Magnetism," Oxford University Press, Oxford, 1985.